Approach to Potential Energy Surfaces by Neural Networks. A Review of Recent Work

ARTICLE *in* INTERNATIONAL JOURNAL OF QUANTUM CHEMISTRY · JUNE 2009

Impact Factor: 1.43 · DOI: 10.1002/qua.22198

Approach to Potential Energy Surfaces by Neural Networks. A Review of Recent Work

DIOGO A. R. S. LATINO,[1,2] RUI P. S. FARTARIA,[1] FILOMENA F. M. FREITAS,[1] JOÃO AIRES-DE-SOUSA,[2] FERNANDO M. S. SILVA FERNANDES[1]

[1]*Department of Chemistry and Biochemistry, Faculty of Sciences, Centre of Molecular Sciences and Materials, Molecular Simulation Group, University of Lisboa, Campo Grande, 1749-016 Lisboa, Portugal*

[2]*Department of Chemistry, Faculty of Sciences and Technology, CQFB and REQUIMTE, New University of Lisboa, 2829-516 Caparica, Portugal*

Received 16 January 2009; accepted 16 February 2009
Published online 3 June 2009 in Wiley InterScience (www.interscience.wiley.com).
DOI 10.1002/qua.22198

ABSTRACT: In the last years, Neural Networks (NNs) turned out as a suitable approach to map accurate Potential Energy Surfaces (PES) from ab initio/DFT energy data sets. PES are crucial to study reactive and nonreactive chemical systems by Monte Carlo (MC) or Molecular Dynamics (MD) simulations. Here we present a review of (a) the main achievements, from the literature, on the use of NNs to obtain PES and (b) our recent work, analyzing and discussing models to map PES, and adding a few details not reported in our previous publications. Two different models are considered. First, NNs trained to reproduce PES represented by the Lennard–Jones (LJ) potential function. Second, the mapping of multidimensional PES to simulate, by MD or MC, the adsorption and self-assembly of solvated organic molecules on noble-metal electrodes, focusing the ethanol/Au (111) interface. In both cases, it is shown that NNs can be trained to map PES with similar accuracy than analytical representations. The results are relevant in the second case, in which simulations by MC or MD require an extensive screening of the interaction sites at the interface, turning the development of analytical functions a nontrivial task as the complexity of the systems increases.
 Int J Quantum Chem 110: 432–445, 2010

Key words: potential energy surfaces; ensembles of feed-forward neural networks; ethanol adsorption on Au (111)

Correspondence to: D. A. R. S. Latino; e-mail: latino@fc.ul.pt.

1. Introduction

The calculation of PES, from ab initio/DFT data, is of high interest in molecular simulations. There are several approaches to fit ab initio/DFT data to analytical functions (e.g., LEPS functions, many body expansions, splines, and semiempirical potentials with adjustable parameters to reproduce experimental and theoretical results). However, these methodologies may show some disadvantages. They might be unable to reproduce, for example, subtle features of complex PES from a limited number of energy points. Moreover, finding suitable analytical functions for complex systems, with many degrees of freedom, appears a nontrivial or, for some cases, even impossible task.

A recent strategy to map PES, with similar or better results than the methods referred to above, is the application of neural networks (NNs).

This article presents an outline of the literature on the latest applications of NNs in this field and a review of some recent results obtained by us, concerning the mapping of PES by NNs in two distinct situations. The first case, reports the mapping of PES (represented by the Lennard-Jones potential) through ensembles of Feed-Forward Neural Networks (EnsFFNNs) and Associative Neural Networks (ASNNs).[1] The second case, assesses an alternative method to map multidimensional PES for the interaction of ethanol and Au (111) interfaces, regarding the simulation of the adsorption and self-assembly of alkylthiols solvated by ethanol [2].

The next sections revise shortly the problems under study and discuss the NNs results and their comparison with the ones from an analytical force field recently proposed by some of us. Section 5 presents the concluding remarks.

2. Neural Networks to Approach PES

In the last years, NNs turned out as an alternative approach for mapping PES from ab initio/DFT energy data sets. In such approach, there are no a priori guesses of analytical functions, that is, neither the functional type (polynomial, exponential, logarithmic, etc.) nor the number and position of the parameters in the model function need to be given. The results come out in tabular form and, after the training, the networks are able to produce, as output, any required number of energy points for numerical interpolations with similar or better accuracy than other representation methods.

A good representation of PES should smoothly connect the asymptotic as well as the most interactive regions of the configurational space. It should accurately represent the true potential energy in the regions for which experimental or theoretical results are available and predict the interaction energies for the regions where such data is not available.

2.1. OUTLINE OF NNS TO APPROACH PES

Feed-Forward Neural Networks (FFNNs) have been applied, for example, to obtain PES for water dimer [3], HCl^+ [4], OH^+ [5], and H^+ [6].

Some authors have compared structural, dynamical, and thermal properties, obtained by Monte Carlo (MC) and Molecular Dynamics (MD) simulations, from NNs-generated PES and analytical functions. Gassner et al. [7] applied FFNNs to reproduce the three body interaction energy of the system H_2O-Al^{3+}-H_2O and assessed the MC radial distribution functions, using an analytical function and the NN-generated PES. A similar study was done by Cho et al. [8] where a polarizable force field for water was developed using NNs and tested in MC simulations.

A more systematic work was performed by Witkoskie et al. [9] who studied the NNs accuracy in terms of some parameters such as the optimal number of neurons and data needed in the training.

More recently, other approaches that combine NNs with other techniques to approach PES more accurately were presented. Raff et al. [10] present a NN/trajectory approach for the determination of PES to be used, for example, in ab initio MD and MC simulations of gas-phase chemical reactions and nanometric cutting. The applicability of the method was demonstrated using the PES of the vinyl-bromide undergoing unimolecular decomposition and the nanometric cutting of silicon. Manzhos and Carrington Jr. [11] developed an approach based on the high-dimensional model representation (HDMR) and NNs to obtain PES. Manzhos et al. [12] present another work where a different NNs approach was used to fit PES. In this approach a first NN was used to fit an approximate PES and then a second and independent NN was used to fit the difference between the true and the approximate PES. The approach was applied in three PES (H_2O, HOOH, and H_2CO).

Malshe et al. [13] presented an approach based on modified novelty sampling and FFNNs to obtain PES to be used in MD simulations of gas-phase chemical dynamics. The approach was applied in the study of the unimolecular dissociation of vinylbromide. Le and Raff [14] also used novelty sampling and FFNNs to approach the PES of the HONO to study their isomerization and dissociation dynamics.

Agrawal et al. [15] applied NNs to fit ab initio data to be used in MD simulations. These authors studied the dissociation of SiO_2. Their work showed the application of NNs to fit ab initio data for an example where the spin multiplicity of the system changes during the dissociation process.

NNs have also been used to obtain PES to study the interaction of molecules with metallic surfaces. The work on reactions in surfaces by Lorenz et al. [16] builds continuous PES for H_2 interacting with a K(2 × 2)/Pd(100) surface and more recently [17] applied NNs to fit six-dimensional PES for H_2 dissociation on the clean and sulfur covered Pd(100) surfaces.

Agrawal et al. [18] used NNs combined with MD to determine reaction probabilities of the reactions occurring in chemical-vapor deposition of carbon dimers on diamond (100) surface. Also, in studies related with metallic surfaces Behler et al. [19] applied NNs to study the interaction of oxygen with Al(111) surface. In this study the authors trained NNs using as input a representation of the Al(111) surface that take into account their symmetry.

Ludwig and Vlachos [20] presented an approach that combines PES construction at the electronic structure level and MD simulations at the atomistic scale for the determination of ab initio PES to be used on classical or quantum mechanical MD simulations of diatomic molecules reacting at metallic surfaces. The H_2/Pt(111) and the H_2/Cu(111) systems were chosen as examples to show the applicability of this approach. In another study related with molecular interaction with metallic surfaces Boyukata et al. [21] applied NNs for the determination of the dissociative chemisorption probabilities for H_2/Ni(111) interaction.

The experiments reviewed here, performed by us, used ensembles of Feed-Forward Neural Networks (EnsFFNNs) and ASNNs. Their advantages and greater generalization ability over single FFNNs have been demonstrated in other problems of modeling and fitting. Both methods are supervised learning techniques but differ in the way how the information is learned and stored. The EnsFFNNs is a memory-less method (after the training all information about the input patterns are implicitly stored in the NN weights but there is no explicit storage of the data in the system) whereas the ASNNs is a combination of memory-less and memory-based methods (the data used to build the models are also stored in a "memory" and the predictions are corrected based on these stored data). The next two subsections will present a small description of these methods.

2.2. FEED-FORWARD NEURAL NETWORKS AND ENSEMBLES OF FEED-FORWARD NEURAL NETWORKS

FFNNs [22] were implemented with one input layer, one hidden layer of neurons, and one output layer. In the input layer and in the hidden layer, an extra neuron (called bias) with a unitary value was also added. A NN converts the input data X, $X = (x_1, x_2, \ldots, x_i, \ldots, x_m)$ into the output data Y, $Y = (y_1, y_2, \ldots, y_i, \ldots, y_n)$. Each neuron of the first layer receives all the input signals of an object and each neuron of one layer is connected to all the neurons of the next layer. These connections are associated with weights that represent the strength of the connection. All neurons j in the network obtain input signals from m neurons, convert these signals to a Net input signal using the expression:

$$\mathrm{Net}_j = \sum_{i=1}^{m} w_{ji} x_i \tag{1}$$

where w_{ji} is the strength of the connection between neuron i and neuron j, and x_i is the input signal from neuron i and transform the Net signal into an output signal:

$$\mathrm{Out} = f(\mathrm{Net}_j) = \frac{1}{1 + \exp(-\gamma \mathrm{Net}_j + \nu)} \tag{2}$$

The function f, called transfer function, is a sigmoidal function.

The networks were trained taking as input, in the first study, the depth of the potential well, ε, the distance at which the potential is equal to 0, σ, and the distance between particles, r. In the second study the distance between the ethanol oxygen atom and the plane of the first layer of the Au (111) surface (r), two angles to describe the orientation of the ethanol to the surface (α and β) and three binary

descriptors to encode the gold adsorption sites (Top, H1, and H2). Corrections of the weights during the training procedure were performed by the Levenberg-Marquardt algorithm [23, 24]. Further details concerning the learning process could be found in Refs. 1 and 2.

An EnsFFNN consists of several independently trained FFNNs, each one contributing with a single prediction [25, 26]. The final prediction for an object, in our case the potential energy, is the average of the outputs from all FFNNs of the ensemble. The experiments were carried out with the ASNN program [27].

2.3. ASSOCIATIVE NEURAL NETWORKS

An ASNN is a combination of a memory-less (ensemble of Feed-Forward Neural Networks) and a memory-based method (K-Nearest Neighbor [28] technique). Full details about this methodology can be found elsewhere [29, 30].

The EnsFFNNs is combined with a memory into a so-called ASNN [29, 30]. In the work reviewed here the memories consists of a list of potential energy points represented by their respective sets of descriptors. An ASNN scheme makes a prediction of the potential energy from: (a) the outputs from the EnsFFNNs and (b) the data in the memory. The experiments here described were carried out with the ASNN program [27].

3. Lennard–Jones Potential

A suitable way to test the accuracy of the properties determined by MC and MD simulation methods, from NNs-generated PES, is to use a simple analytical potential function from which an arbitrary number of energy points can always be worked out. The LJ analytical PES, for example, from which a huge amount of physical properties has been calculated along the past years, is a convenient potential to perform the experiments. If the test results are accurate enough, then experiments toward more complex and multidimensional PES can be devised.

The main goal of this work was precisely to train NNs for reproducing PES represented by the Lennard-Jones potential, and then to assess the accuracy of the method by comparing the simulation results obtained from the NNs tables and the analytical PES. EnsFFNNs [25, 26] and ASNNs [29, 30] were the automatic learning methods used to estimate the full energy surface.

The experiments involved two main steps. In the first, training sets with different numbers of energy points were generated for 15 differently parameterized LJ potentials:

$$u(r) = 4\varepsilon\left\{\left(\frac{\sigma}{r}\right)^{12} - \left(\frac{\sigma}{r}\right)^{6}\right\} \tag{3}$$

where ε is the depth of the potential well, σ is approximately the molecular diameter (the distance at which the potential is equal to zero), and r is the distance between particles. A test set was generated with the parameters for argon. EnsFFNNs and ASNNs were used to set up the relation between the input (parameters σ, ε, and the distance between particles, r) and the output (potential energy). In the second step, the NN-generated PES of argon, in tabular form, was used in MD simulations and the evaluated thermal, structural, and dynamic properties were compared with the ones obtained from the analytical PES for argon, also in tabular form to avoid errors due to the interpolations. Experiments were also performed to assess the ability of an ASNN trained with a small number of points to improve the generated PES by using different memories with more points, or by retraining with more points.

3.1. DATASET GENERATED BY LJ POTENTIAL

EnsFFNNS and ASNNs are supervised learning methods and, therefore, they need a set of pairs to learn: the inputs and the targets. This study had three inputs: ε, σ, and r, and one target (output) the potential energy, $u(r)$.

The LJ parameters used for 16 substances [31, 32] are listed in Table I. Training sets, with different number of energy points, were generated with the analytical expression for the 15 PES. Because in MD simulations the potential energy calculated with distances between particles shorter than $0.5 \times \sigma$ and larger than $2.5 \times \sigma$ has no influence on the results the energy points used to train and test the models were generated between these values with different intervals for the five training sets and with an interval of $\sim 7.246 \times 10^{-4}$ Å for the test set. The number of objects in each training set was 1,312, 442, and 267.

TABLE I

Lennard-Jones parameters for the substances used in the training and test of NNs.

	ε/K	σ/pm
He	10.22	258.0
C_2H_2	209.11	463.5
C_2H_4	200.78	458.9
C_2H_6	216.12	478.2
C_6H_6	377.46	617.4
CCl_4	378.86	624.1
CO_2	201.71	444.4
F_2	104.29	357.1
Kr	154.87	389.5
N_2	91.85	391.9
O_2	113.27	365.4
Xe	213.96	426.0
Ne	35.7	279
CH_4	137	382
Cl_2	296.27	448.5
Ar	111.84	362.3

Because of the steep varying nature of the first part of the potential, and the requirement that the input and output of NNs is normalized between 0.1 and 0.9, each PES of the training set was divided in one part with r between $0.5 \times \sigma$ and σ, and a second part with r from σ to $2.5 \times \sigma$. Accordingly, each data set was divided into two subsets, and each one was used to separately train NNs. Each network makes predictions for one part of the potential. After this division, the training sets had the following number of points (in each part of the curve): 1,312 (315 + 997), 442 (162 + 280), and 390 (162 + 228).

3.2. MD SIMULATIONS

The EnsFFNN and ASNN models obtained using different training sets (each containing a different number of points) were separately applied to generate an external table with 1,003 energy points for argon. These external tabular PES were then used in MD simulations with cubic periodic boundary conditions. The MD program reads and interpolates the potential energy generated by NNs from the external tables. Finally, the simulation results were compared with the ones from the LJ analytical function.

The simulations were performed in the NVT ensemble (damped-force method [33]) at different thermodynamic conditions, with a time step of 1.0×10^{-14} s for the numerical integration of Newton's equations of motion (using Verlet's leap-frog algorithm [33]) and 50,000 time steps for the equilibration and production runs.

3.3. GENERATION OF PES BY NNS USING THE LJ POTENTIAL

The comparison between the LJ data and the predictions of the models for the different experiments were analyzed in terms of the root mean square error (RMSE):

$$\mathrm{RMSE} = \sqrt{\frac{\sum_{i=1}^{n}[(Y_{\mathrm{calc}} - Y_{\mathrm{exp}})^2]}{n}} \tag{4}$$

where Y_{calc} is the predicted value, Y_{exp} is the target value and n is the number of objects, or using the mean absolute error (MAE):

$$\mathrm{MAE} = \frac{\sum_{i=1}^{n}|Y_{\mathrm{calc}} - Y_{\mathrm{exp}}|}{n} \tag{5}$$

where Y_{calc} is the predicted value, Y_{exp} is the target value and n is the number of objects.

The models for the first part of the curve ($0.5 \times \sigma < r < \sigma$) were trained with three different data sets. The results using ASNNs were in general better than the ones using EnsFFNNs, particularly for the test set and for training sets with fewer points. The errors were in all cases lower than 5% for the test set.

Table II shows the results for the second part of the curve (r between σ and $2.5 \times \sigma$) for three different training sets (997, 280, and 171 energy points).

Although the results for the test set using the model trained with 997 energy points were considerably better the others two examples showed an acceptable MAE. Reducing the number of energy points from 280 to 171 resulted in a significant increase of the RMSE from 0.135 to 0.639. This limit of energy points was considered as the minimum number of energy points required for an ASNNs to learn, properly, the relation between the LJ parameters and the potential energy. Full details of the experiments performed with different number of neurons in the hidden layer and with training sets

TABLE II

Mean Absolute Error (MAE) for training and test sets using EnsFFNNs and ASNNs trained with different sets for the second part of the PES (σ < r < 2.5 × σ).

NN Type	Data sets	MAE[a]/K		
		997	280	171
EnsFFNNs	Learning	0.116	0.601	0.899
	Validation	0.281	1.724	2.786
	LOO	0.269	1.809	3.092
	Test	0.096	0.277	1.022
ASNNs	Learning	0.109	0.562	0.796
	Validation	0.237	1.409	2.469
	LOO	0.227	1.497	2.758
	Test	0.050	0.135	0.639

[a] 997, 280, 171 are the number of energy points used in training.

of different dimensions could be found elsewhere [1].

Figure 1 shows the NN-generated PES for argon and respective comparison with the PES for argon from LJ function. The NN-generated PES were in good agreement with those obtained from the LJ function in all regions of the curve. The region that present worse results is near σ (where the potential is zero) with an average error of 8% for 25 energy points.

3.4. PROPERTIES FROM MOLECULAR DYNAMICS SIMULATIONS

Table III shows the properties calculated from MD simulations where the errors are measured relatively to the results obtained using a tabular PES of argon using the LJ function.

The energies and pressures were in good accordance with the values worked out from the LJ function with errors less than 1% unless for the training set with 267 energy points.

The heat capacities and diffusion coefficient presented errors between 1 and 2%. The ASNN model that gives better results was the one worked out with 442 energy points (162 + 280) showing that the number of energy points used and the overall fitting of the argon curve was enough for obtaining good results using a training set with 1,312 or 442 energy points. In the last experiment, with only 267 energy points a significant increase in the errors in some properties was observed.

Experiments were performed with training sets of different dimensions and at different thermodynamic conditions (different points of the argon phase diagram) to check out the impact in the accuracy of the results. The results showed that the accuracy is almost unchanged for the most part of the experiments. More details concerning these experiments could be found elsewhere [1].

Figure 2 shows the radial distribution functions (rdf) and velocity autocorrelation functions (vcf) that were in excellent agreement with those from LJ function.

Finally, a situation where new data became available and was subsequently incorporated in the ASNNs memory has been simulated. The ASNN methodology allows the incorporation of new data in the memory after the training is finished without requirement of retraining making possible to improve predictions. This feature could be applied in situations where the data is calculated by ab initio methods and becomes available only gradually.

Such possibility was simulated in a series of experiments where a ASNN was initially trained with a small number of energy points and then more energy points were incorporated in the memory without retrain. The results were then compared with those obtained by training the ASNN with the same number of energy points that were incorporated in the memory. The experiments showed that it is possible to train a ASNN with a small number of energy points and improve the accuracy of the predictions using memories with

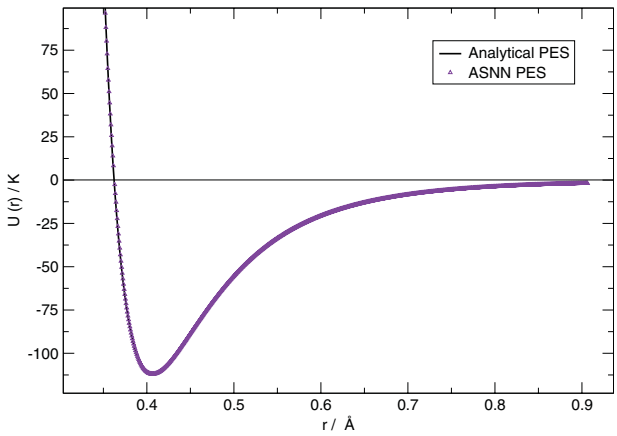

FIGURE 1. Potential energy of argon generated by ASNN, trained with 442 (162 + 280) energy points, compared with the analytical PES. [Color figure can be viewed in the online issue, which is available at www.interscience.wiley.com.]

TABLE III

Thermal and dynamic properties evaluated in MD simulations (NVT ensemble, $N = 256$, $T = 1.0$, $\rho = 0.85$) using the PES of argon generated by ASNNs.

Properties	Analytical Function	NN generated PES		
		1312	442	267
E	−4.322	−4.341 (0.44%)	−4.324 (0.03%)	−4.422 (2.31%)
K	1.500	1.500 (0.00%)	1.500 (0.00%)	1.500 (0.00%)
U	−5.822	−5.841 (0.33%)	−5.824 (0.03%)	−5.846 (0.41%)
p	1.936	1.922 (0.71%)	1.936 (0.01%)	1.847 (4.62%)
C_v	2.519	2.564 (1.78%)	2.544 (1.02%)	2.570 (2.03%)
DC/cm^2s^{-1}	2.635E-5	2.581E-5 (2.04%)	2.607E-5 (1.07%)	2.555E-5 (3.05%)

T, temperature; ρ, density; E, total energy; K, kinetic energy; U, potential energy; p, pressure; C_v, heat capacity; (all in reduced units). DC, diffusion coefficient.
Within the parentheses are the errors of the properties using NN-generated PES relatively to the results using the analytical function. 1,312, 442, 267 are the number of energy points used in training.

more data. The results were similar to the ones obtained by ASNNs trained from the beginning with all data in each training set. The method not only uses global knowledge stored implicitly in the NNs weights of the ensemble but also local knowledge retrieved from the most similar objects in the memory.

4. The Ethanol/Au(111) Interface

The adsorption and spontaneous organization of organic molecules on metallic surfaces give rise to films of organized and stable monolayers, known as Self-Assembled Monolayers (SAMs). The modification of metallic surfaces properties by SAMs allows, for example, photovoltaic, biosensing, and corrosion protection developments.

SAMs can be produced using different types of molecules and substrates. Because of the well-known chemical affinity between sulfur and gold, alkane chains (with 10 or more methylene units) and a thiol (SH) head group are used with Au surfaces. These species have the ability of create dense monolayers when the thiol molecules adsorb onto gold with the tail chains pointing outwards the surface. Moreover, the tail chain can be functionalized after the formation of the SAMs, by the chemical insertion of specific functional groups or molecules.

To investigate these processes by molecular simulation, the determination of the PES of the systems is crucial. They should describe the interactions between the molecular species present in the liquid

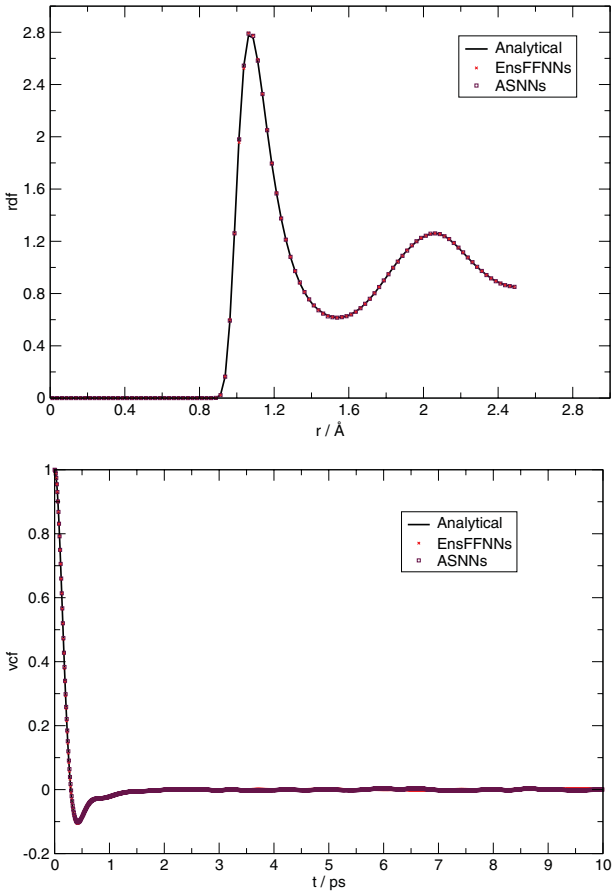

FIGURE 2. Radial distribution functions (top graphic) and Velocity autocorrelation functions (bottom graphic) for argon obtained in MD simulations using the PES generated by NNs (EnsFFNN and ASNN trained with 442 energy points) compared, respectively, with the rdf and vcf from the analytical function. [Color figure can be viewed in the online issue, which is available at www.interscience.wiley.com.]

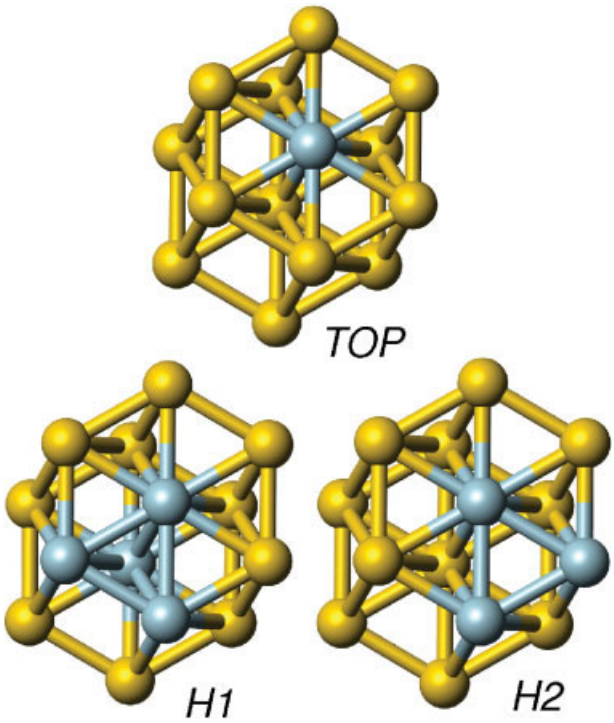

FIGURE 3. Gold sites, Top, H1 and H2, chosen to set up the ethanol-Au(111) PES. [Color figure can be viewed in the online issue, which is available at www.interscience.wiley.com.]

phase as well as the interactions of those species with the electrodes.

The main objective was to assess an alternative to the analytical force field previously developed [34], to map multidimensional PES for the interaction of ethanol and Au (111) surfaces regarding the simulation of the adsorption and self-assembly of alkylthiols solvated by ethanol.

EnsFFNNs [25, 26] was the automatic learning method used to establish the relationship between the input (two orientation angles describing the molecular orientation relatively to the surface, the distance between the ethanol oxygen atom and the plane of the first layer of the Au (111) surface, and three binary descriptors to encode the gold adsorption sites) and the output (potential energy). The training sets contain energy values of the ethanol at different distances to the surface over three adsorption sites in seven molecular orientations. The models were assessed by internal and external test sets.

The training had been performed with the DFT data of Fartaria et al. [34] An additional set of DFT energy points has been calculated, at six orientations, to test the models in regions of the PES not considered in the training.

The results were compared with the values from DFT calculations and an analytical force field [34]. The NNs-generated PES for each gold site, in 3D representations, were analyzed. Further details are fully described elsewhere [2].

4.1. DFT CALCULATIONS

The theory level chosen to calculate the interaction energy of ethanol/Au (111) was the hybrid B3LYP method [35, 36] with the LanL1MB basis set [37] applied to the gold atoms and the 6-31G basis set [38] for the H, C, and O atoms.

A cluster of 14 Au atoms, to represent the surface, and one ethanol molecule, in the optimized gas-phase geometry, has been used to model the

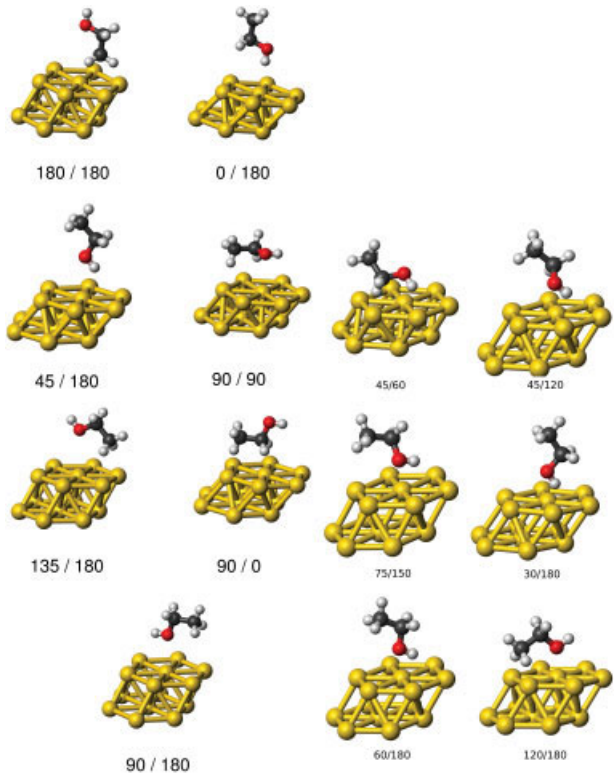

FIGURE 4. Molecular orientations of the ethanol molecule relative to the Au(111) surface used in the training and test sets (notation: α/β, see text). [Color figure can be viewed in the online issue, which is available at www.interscience.wiley.com.]

TABLE IV

Errors of the minimum of each curve for each orientation and adsorption site of the training and test sets.

Orientation		Distance	Potential Energy		$-U$/kJmol^{-1}
α/deg.	β/deg.	O-surf. r/Å	DFT	Anal. Funct.	EnsFFNNs
Top site					
0	180	3.54	7.76	8.7 (0.94)	7.96 (0.20)
135	180	4.07	5.87	6.7 (0.83)	6.15 (0.28)
180	180	6.0	1.37	1.2 (0.17)	1.78 (0.41)
45	180	3.3	9.04	15.0 (5.96)	9.13 (0.09)
90	0	5.5	2.32	1.5 (0.82)	2.38 (0.06)
90	180	2.67	19.03	19.25 (0.22)	18.17 (0.86)
90	90	3.54	11.77	10.4 (1.37)	11.95 (0.18)
45	60	3.79	7.0	8.78 (1.78)*	−2.70 (9.70)*
45	120	3.37	9.81	14.14 (4.33)*	5.65 (4.16)*
75	150	2.81	15.91	18.85 (2.94)*	17.09 (1.18)*
30	180	3.37	7.75	13.36 (5.61)*	8.10 (0.35)*
60	180	3.17	11.52	16.63 (5.11)*	11.93 (0.41)*
120	180	3.17	11.84	12.13 (0.29)*	11.49 (0.35)*
H1 site					
0	180	3.3	13.14	10.7 (2.44)	12.93 (0.21)
135	180	4.29	4.34	5.5 (1.16)	3.96 (0.34)
180	180	6.04	1.35	0.9 (0.45)	1.51 (0.16)
45	180	2.87	16.42	13.3 (3.12)	14.61 (1.81)
90	0	5.57	2.35	1.4 (0.95)	2.46 (0.11)
90	180	2.87	12.80	15.5 (2.7)	13.91 (1.11)
90	90	3.87	5.99	7.1 (1.11)	6.03 (0.04)
45	60	3.79	6.69	7.20 (0.51)*	3.07 (3.62)*
45	120	3.17	12.50	13.03 (0.53)*	7.48 (5.02)*
75	150	2.81	12.58	15.46 (2.88)*	12.82 (0.32)*
30	180	3.17	15.59	12.76 (2.83)*	14.86 (0.73)*
60	180	2.81	16.71	14.34 (2.37)*	14.68 (2.03)*
120	180	3.58	6.64	10.43 (3.79)*	6.43 (0.21)*
H2 site					
0	180	3.3	10.46	9.8 (0.66)	10.32 (0.14)
135	180	4.2	5.08	5.3 (0.22)	4.96 (0.12)
180	180	6.04	1.48	1.0 (0.48)	1.42 (0.06)
45	180	3.08	11.82	12.7 (0.88)	11.39 (0.43)
90	0	5.37	2.33	1.4 (0.93)	2.37 (0.04)
90	180	2.67	15.07	14.7 (0.37)	14.86 (0.21)
90	90	3.87	5.75	7.1 (1.35)	6.03 (0.28)
45	60	4.02	4.44	6.55 (2.11)*	2.11 (2.33)*
45	120	2.99	10.61	12.09 (1.48)*	3.96 (6.65)*
75	150	2.81	13.78	14.50 (0.72)*	13.24 (0.54)*
30	180	3.17	10.73	12.19 (1.46)*	10.54 (0.19)*
60	180	2.81	13.09	13.37 (0.28)*	12.59 (0.50)*
120	180	3.37	8.55	10.61 (2.06)*	7.88 (0.67)*

EnsFFNNs - Training with 366 energy points, tested with 414 energy points.
For all orientations the results from the test set are marked with *.

ethanol/Au (111) PES. Figure 3 shows the three adsorption sites that has been selected to study the ethanol-gold interactions - top (Top) where the oxygen atom of ethanol approaches the surface directly over a gold atom of the first layer, hollow 1 (H1) that corresponds to a hcp (hexagonal closed packed) site and hollow 2 (H2) corresponding to a fcc (face-centered cubic) site.

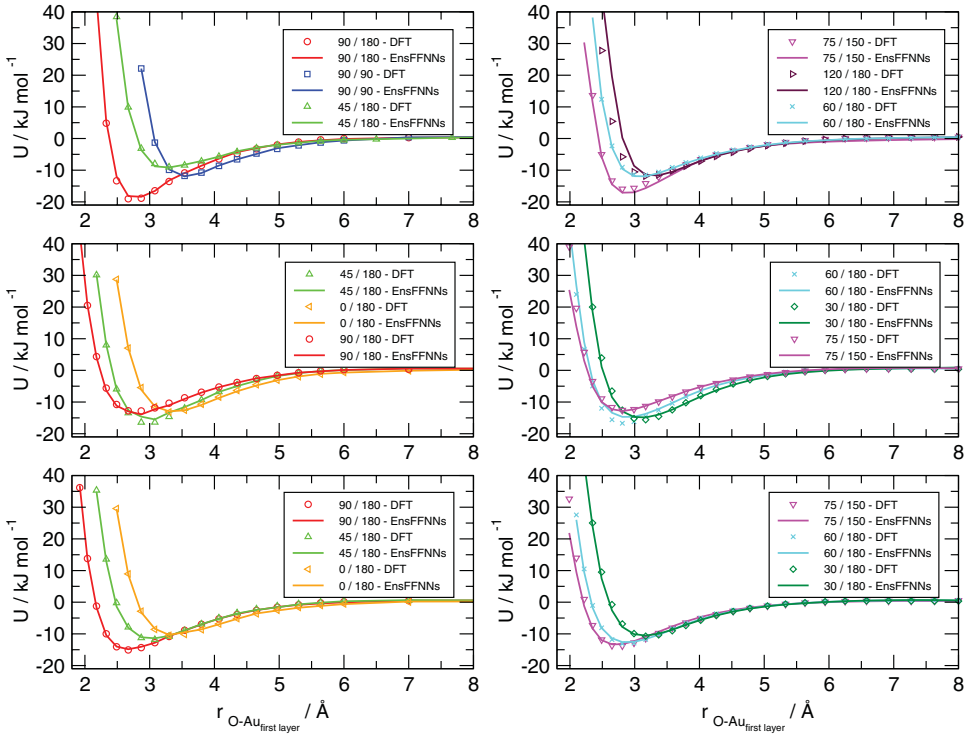

FIGURE 5. Ethanol-Au $(111)_{14}$ potential energy curves by DFT and EnsFFNNS for the Top, H1 and H2 sites (from top to bottom, respectively) from the training (left) and test (right) set. [Color figure can be viewed in the online issue, which is available at www.interscience.wiley.com.]

The ethanol/Au $(111)_{14}$ interaction energy, as a function of the distance and orientation of ethanol to the Au (111) surface, was defined by:

$$U_{\text{ethanol–Au(111)}_{14}}(r,\alpha,\beta) = U_{\text{Au(111)}_{14}+\text{ethanol}}(r,\alpha,\beta) - U_{\text{Au(111)}_{14}} - U_{\text{ethanol}} \quad (6)$$

where $U_{\text{Au(111)14+ethanol}}$ is the energy of the system composed by the ethanol molecule and the cluster; $U_{\text{Au(111)14}}$ and U_{ethanol} are the energies of the isolated cluster and ethanol molecule; r is the distance from the ethanol oxygen atom to the plane of the first layer of the Au(111) surface; α is the angle between the O—H bond and the normal to the surface and β is the angle between the plane H—O—C and the plane H—O-normal to the surface (both angles in degrees). The orientations for the ethanol molecule has been selected to span a wide range of situations. Figure 4 shows the molecular orientations used for training and test the NNs. For each orientation the $U_{\text{ethanol}-\text{Au(111)14}}$ energy was evaluated for several values of r, along the interval 0–10 Å. Some DFT results have also been fitted to an analytical force field. The calculations had been performed with Gaussian 98 package [39]. The full details of the DFT calculations and force field are described elsewhere [34].

4.2. MAPPING OF PES OF ETHANOL/AU(111)

Experiments were performed to check out the impact of the number of hidden neurons, and the size of the ensembles, on the accuracy of the models. The RMSE decreased from ~8 kJ mol^{-1} for networks with two hidden neurons to ~5 kJ mol^{-1} for networks with more than five hidden neurons (in ensembles of 15 networks). Networks with more than 10 hidden neurons did not present significant improvement and increases computational requirements. Concerning the impact of the number of networks in the ensemble, using more than 10 networks did not show a significant improvement in the predictions.

The comparison between the minima of the potential energy for each orientation of the ethanol

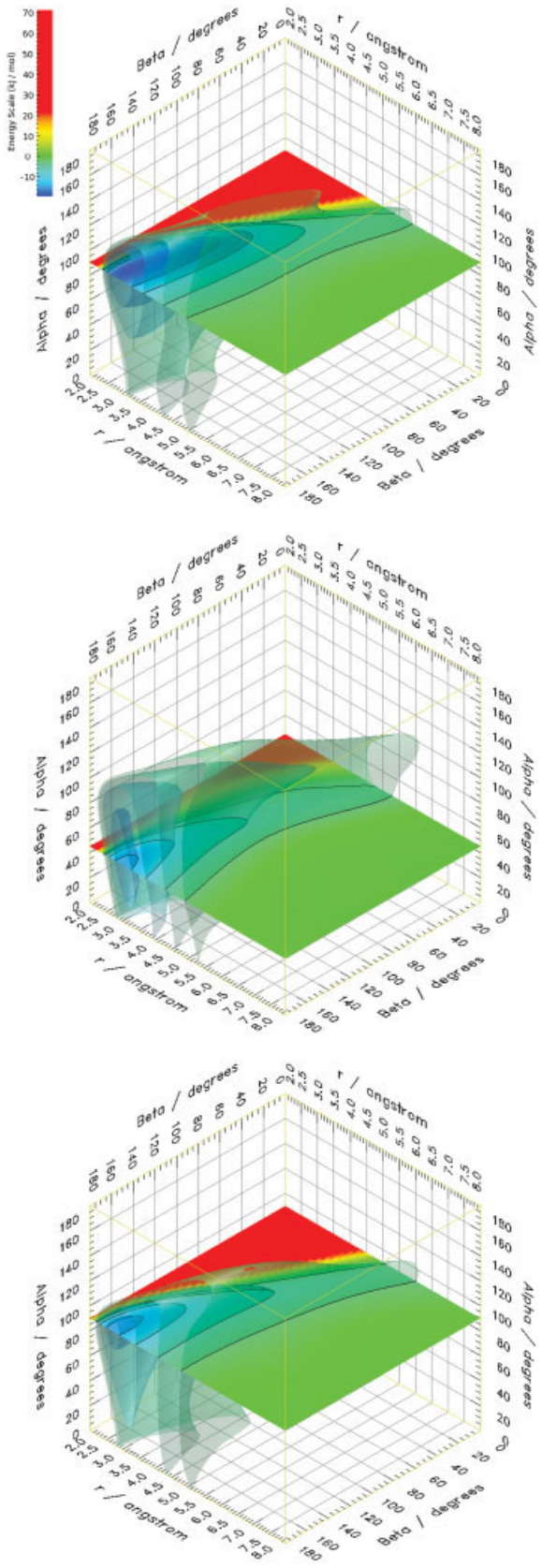

molecule and adsorption sites, at the same distance from, DFT calculations, EnsFFNNs, and analytical function (previously developed) are presented in Table IV.

The results for the training set were, in general, in good accordance with DFT data. Only two cases presented absolute errors higher than 1 kJ mol^{-1}. The results for the test set showed the same level of accuracy as those from the training set. The only exceptions were the 45/60 and 45/120 orientations that presented considerable errors in all adsorption sites studied. The 45/60 orientation for top site presented a positive binding energy. This results can be, presumably, explained by the fact that the β angle was not well represented in the training set where only two orientations were different of 180°. The EnsFFNNs provided in the most part of the orientations more accurate predictions than the analytical function with exception of the above cited orientations.

Figure 5 shows the entire curves for the three most attractive orientations on each site for training and test set with values from EnsFFNNs and DFT calculations. Considering all orientations the most significant deviations from DFT data were in the repulsive part of the curves. However, the repulsive part of the curve is less important taking in consideration that the probability of this part of the curve becoming sampled in the course of a simulation is very low. The 60/180 orientation on H1 site presented a deviation of ~2 kJ mol^{-1} in the attractive part of the curve.

After the learning procedure, 83,509 energy points have been predicted by the established models for distances of the ethanol to the surface between 2 and 8 $\AA$, with an interval of 0.1 $\AA$, and for α and β angles between 0 and 180°, with an interval of 5°. Each site was treated separately. Figure 6 displays the PES for the Top, H1, and H2 sites in a 3D representation.

The cutting planes in each representation included energy minimas for the different sites, for

FIGURE 6. PES of ethanol over the Top, H1 and H2 sites. Four isoenergetic surfaces are displayed at −14, −10, −5, and −2 kJ mol^{-1}. The plane cuts the surfaces at α = 90°, 45°, and 90° for Top, H1, and H2, respectively. The isoenergetic lines correspond to the energies −14, −10, −5, and −2 kJ mol^{-1}. The colored bar represents the energy scale. [Color figure can be viewed in the online issue, which is available at www.interscience.wiley.com.]

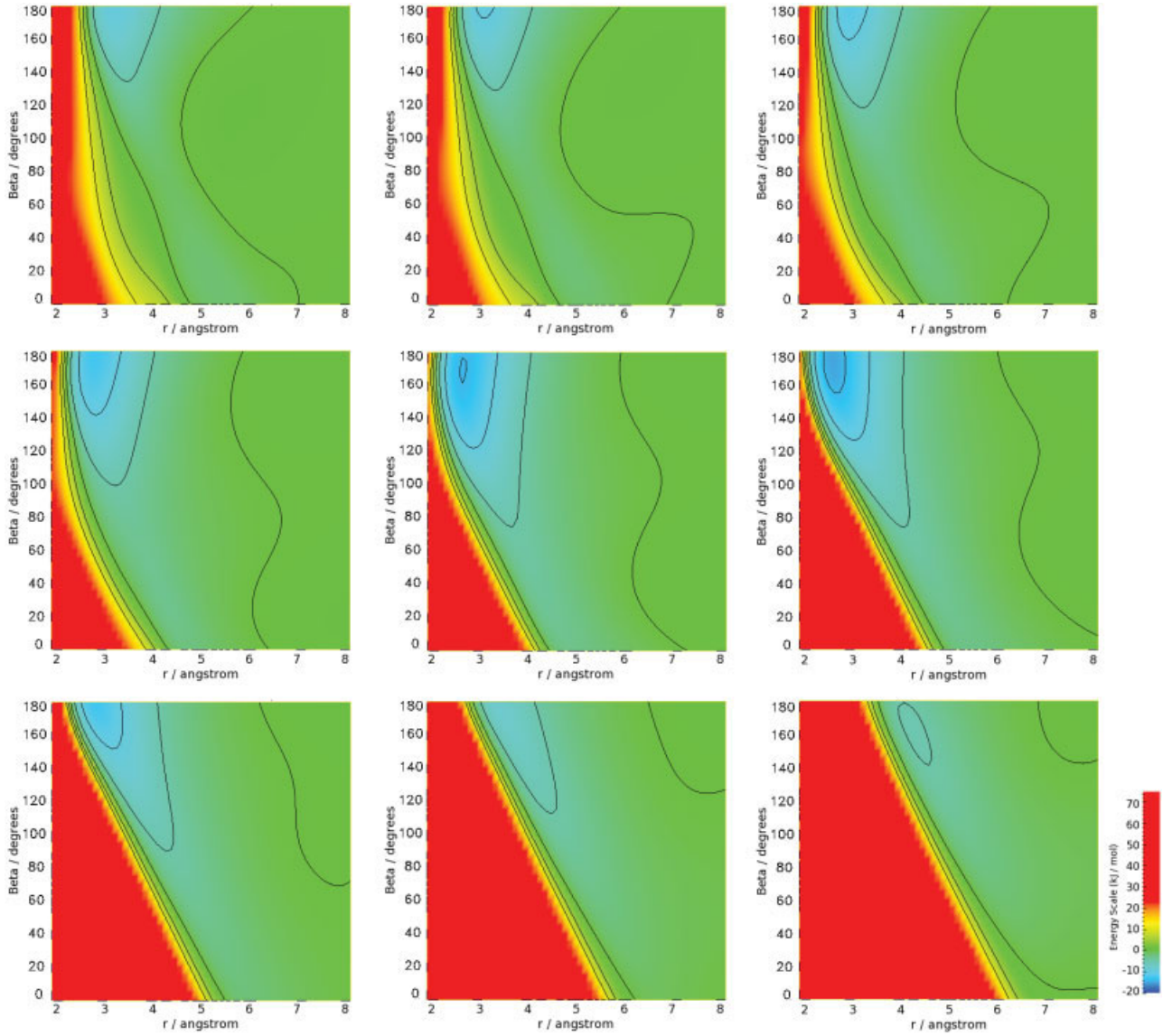

FIGURE 7. PES projections for the H2 site. First row, from the left to right, projections at $\alpha = 15°, 30°, 45°$; second row, from left to right, projections at $\alpha = 60°, 75°, 90°$; third row, from the left to right, $\alpha = 105°, 120°, 135°$. The isoenergetic lines correspond to potential energy of -14, -10, -5, 0, 5, and 10 kJ mol^{-1}. The colored bar represents the energy scale. [Color figure can be viewed in the online issue, which is available at www.interscience.wiley.com.]

example in Top site at $\beta = 180°$ and $r = 2.8$ Å and in H1 site at $\beta = 180°$ and $r = 2.9$ Å (see Table IV). The isoenergetic lines showed the energy dependence on the distance and the β angle for the corresponding α angle.

Figure 7 illustrates PES projections for the H2 site where can be observed the variation of the potential energy according to angle β and the distance of the molecule to the surface for nine values of angle α ($\alpha = 15°, 30°, 45°, 60°, 75°, 90°, 105°, 120°$, and 135°). The PES projections are in accordance with the calculated DFT data both for training and test except for the regions of the test set, 45/60 and 45/120, previously discussed. Nonetheless with this type of projections an easy visual analysis of the behavior of the PES can be performed according the orientations angles and the distance. It can be concluded that the NN-generated PES smoothly

connect the different regions of the PES used in the training generating an accurate PES for the interaction of ethanol/Au(111).

The lesser accurate predictions of the NN-generated PES in some surface regions could be attributed not to some limitations of the network training but to the limited data set of energy points. Although the limited number of orientations in the training set the NN ability to mapping multidimensional data was demonstrated by the accurate predictions for the most part of the orientations in the external test set.

Further experiments have been performed with different training parameters (initial weights), new partitions of the data and training with all data available without external test set. The results showed that using different partitions the accuracy were, in the overall, similar. The use of new partitions of the data can be useful to improve the predictions for the 45/60 and 45/120 orientations but other orientations were not so well predicted. These results indicate again that the data available did not cover the configuration space well enough, leading to large errors for some orientations in the space regions that were not so well represented in the training sets. Further details concerning these experiments are described elsewhere [2].

5. Final Remarks

Part of our work concerned with the application of NNs to approach PES has been reviewed, adding some graphical details not reported in our previous publications. The results of the first study show that NN can be trained to map PES with enough accuracy to be used in molecular simulations. These results, complemented by the second study, indicate that NNs can be considered a suitable alternative to the development of analytical functions. The experiments revised here suggest that NNs are able to reproduce PES with similar or better accuracy than analytical functions even for complex systems.

The NNs-PES obtained for the ethanol/Au (111) interaction have to be tested in molecular simulations. The test will be carried out using the tabular potential energies, predicted by the NNs, for working out thermal, structural and dynamical properties to be compared with the preliminary Monte Carlo simulation values already obtained from the analytical function [34]. Once the networks are well trained they are able to produce, as output, any required number of energy points for numerical interpolations. However, before a full simulation test can be performed, based on NNs data, a much finer screening of the gold interaction sites, and ethanol orientations, is needed. Work is in progress to obtain DFT results for sites other than the Top, H1 and H2 and train models taking in consideration the symmetry of the Au(111) surface. Such results will certainly increase the extension and accuracy of the NNs mappings. Nonetheless, the conclusions from these experiments do not depend on the choice of the system and model but rather indicate that NNs offer an alternative to be used in Monte Carlo and molecular dynamics simulations. As for molecular dynamics, which usually require continuously differentiable potentials, the interpolation routines may, however, slow down the simulations.

ACKNOWLEDGMENT

The authors acknowledge Fundação para a Ciência e Tecnologia (FCT, Portugal) for finan- cial support and Dr. Igor Tetko who made available the software to implement EnsFFNNs and ASNNs.

References

1. Latino, D. A. R. S.; Freitas, F. F. M.; Aires-de-Sousa, J.; Fernandes, F. M. S. S. Int J Quantum Chem 2007, 107, 2120.
2. Latino, D. A. R. S.; Fartaria, R. P. S.; Freitas, F. F. M.; Aires-de-Sousa, J.; Fernandes, F. M. S. S. J Electroanal Chem 2008, 624, 109.
3. No, K. T.; Chang, B. H.; Kim, S. Y.; Ihon, M. S.; Scheraga, H. A. Chem Phys Lett 1997, 271, 152.
4. Prudente, F. V.; Neto, J. J. S. Chem Phys Lett 1998, 287, 585.
5. Bittencourt, A. C. P.; Prudente, F. V.; Vianna, J. D. M. Chem Phys 2004, 297, 153.
6. Filho, T. M. R.; Oliveira, Z. T.; Malbouisson, L. A. C.; Gargano, R.; Neto, J. J. S. Int J Quantum Chem 2003, 95, 281.
7. Gassner, H.; Probst, M.; Lauenstein, A.; Hermansson, K. J Phys Chem A 1998, 102, 4596.
8. Cho, K. H.; No, K. T.; Scheraga, H. A. J Mol Struct 2002, 641, 77.
9. Witkoskie, J. B.; D. J. Doren, D. J. J Chem Theory Comput 2005, 1, 14.
10. Raff, L. M.; Malshe, M.; Hagan, M.; Doughan, D. I.; Rockley, M. G.; Komanduri, R. J Chem Phys 2005, 122, 084104.
11. Manzhos, S.; Carrington, T., Jr. J Chem Phys 2006, 125, 084109.
12. Manzhos, S.; Wang, X.; Dawes, R.; Carrington, T., Jr. J Phys Chem A 2006, 110, 5295.
13. Malshe, M.; Raff, L. M.; Rockley, M. G.; Hagan, M.; Agrawal, P. M.; Komanduri, R. J Chem Phys 2007, 127, 134105.

14. Le, H. M.; Raff, L. M. J Chem Phys 2008, 128, 194310.
15. Agrawal, P. M.; Raff, L. M.; Hagan, M. T.; Komanduri, R. J Chem Phys 2006, 124, 134306.
16. Lorenz, S.; Grob, A.; Sheffler, M. Chem Phys Lett 2004, 395, 210.
17. Lorenz, S.; Sheffler, M.; Grob, A. Phys Rev B 2006, 73, 115431.
18. Agrawal, P. M.; Samadh, A. N. A.; Raff, L. M.; Hagan, M.; Bukkapatnam, S. T.; Komanduri, R. J Chem Phys 2005, 123, 224711.
19. Behler, J.; Lorenz, S.; Reuter, K. J Chem Phys 2007, 127, 014705.
20. Ludwig, J.; Vlachos, D. G. J Chem Phys 2007, 127, 154716.
21. Boyukata, M.; Kocyigit, Y.; Guvenc, Z. B. Croat Chem Acta 2008, 81, 305.
22. Zupan, J.; Gasteiger, J. Neural Networks in Chemistry and Drug Design; Wiley-VCH: Weinheim, 1999.
23. Press, W. H.; Teukolsky, S. A.; Vetterlung, W. T.; Flannery, B. P. Numerical Recipes in C, 2nd ed.; Cambridge University Press: New York, 1994.
24. Shepherd, A. J. Second Order Methods for Neural Networks; Springer-Verlag: London, 1997.
25. Agrafiotis, D. K.; Cedeno, W.; Lobanov, V. S. J Chem Inf Comput Sci 2002, 42, 903.
26. Dietterich, T. G. The Handbook of Brain Theory and Neural Networks; Arbib, M. A., Ed.; MIT Press: Cambridge, MA, 2002; p 405.
27. VCCLAB, Virtual Computational Chemistry Laboratory, Available at: http://www.vcclab.org 2005.
28. Dasarthy, B. Nearest Neighbor (NN) Norms; IEEE Computer Society Press: Washington, DC, 1991.
29. Tetko, I. V. J Chem Inf Comput Sci 2002, 42, 717.
30. Tetko, I. V. Neural Process Lett 2002, 16, 187.
31. Cuadros, F.; Cachadina, J.; Ahmuda, W. Mol Eng 1996, 6, 319.
32. Hirschfelder, J. O.; Curtiss, C. F.; Bird, R. B. Molecular Theory of Gases and Liquids; Wiley: New York, 1954.
33. Allen, M. P.; Tildesley, D. J. Computer Simulation of Liquids; Claredon Press: Oxford, 1987.
34. Fartaria, R. P. S.; Freitas, F. F. M.; Fernandes, F. M. S. S. Int J Quantum Chem 2007, 107, 2169.
35. Becke, A. D. J Chem Phys 1993, 98, 5648.
36. Becke, A. D. J Chem Phys 1993, 98, 1372.
37. Hay, P. J.; Wadt, W. R. J Chem Phys 1985, 82, 270.
38. Hehre, W. J.; Ditchfield, R.; Pople, J. A. J Chem Phys 1972, 56, 2257.
39. Frisch, M. J.; Trucks, G. W.; Schlegel, H. B.; Scuseria, G. E.; Robb, M. A.; Cheeseman, J. R.; Zakrzewski, V. G.; Montgomery, J. A.; Stratmann, R. E.; Burant, J. C.; Dapprich, S.; Millam, J. M.; Daniels, A. D.; Kudin, K. N.; Strain, M. C.; Farkas, O.; Tomasi, J.; Barone, V.; Cossi, M.; Cammi, R.; Mennucci, B.; Pomelli, C.; Adamo, C.; Clifford, S.; Ochterski, J.; Petersson, G. A.; Ayala, P. Y.; Cui, Q.; Morokuma, K.; Malick, D. K.; Rabuck, A. D.; Raghavachari, K.; Foresman, J. B.; Cioslowski, J.; Ortiz, J. V.; Stefanov, B. B.; Liu, G.; Liashenko, A.; Piskorz, P.; Komaromi, I.; Gomperts, R.; Martin, R. L.; Fox, D. J.; Keith, T.; Al-Laham, M. A.; Peng, C. Y.; Nanayakkara, A.; Gonzalez, C.; Challacombe, M.; Gill, P. M. W.; Johnson, B. G.; Chen, W.; Wong, M. W.; Andres, J. L.; Head-Gordon, M.; Replogle, E. S.; Pople, J. A. Gaussian 98 Gaussian Inc. Pittsburgh PA, 1998.